J. Fluid Mech. (1970), *vol.* 42, *part* 3, *pp.* 471–489
Printed in Great Britain

Numerical solutions for steady flow past a circular cylinder at Reynolds numbers up to 100

By S. C. R. DENNIS AND GAU-ZU CHANG
Department of Applied Mathematics, University of Western Ontario, London, Canada

(Received 27 June 1969 and in revised form 3 February 1970)

Finite-difference solutions of the equations of motion for steady incompressible flow around a circular cylinder have been obtained for a range of Reynolds numbers from $R = 5$ to $R = 100$. The object is to extend the Reynolds number range for reliable data on the steady flow, particularly with regard to the growth of the wake. The wake length is found to increase approximately linearly with R over the whole range from the value, just below $R = 7$, at which it first appears. Calculated values of the drag coefficient, the angle of separation, and the pressure and vorticity distributions over the cylinder surface are presented. The development of these properties with Reynolds number is consistent, but it does not seem possible to predict with any certainty their tendency as $R \to \infty$. The first attempt to obtain the present results was made by integrating the time-dependent equations, but the approach to steady flow was so slow at higher Reynolds numbers that the method was abandoned.

1. Introduction

Numerical solutions for two-dimensional flow past a circular cylinder can be divided into two broad classes. First, there are those obtained by integrating the equations of steady motion. Thom (1928) gave the first solution at $R = 10$, where R is the Reynolds number based on the diameter of the cylinder. Subsequently Thom (1933) gave a solution at $R = 20$ and Kawaguti (1953*b*), Apelt (1961) have both obtained solutions at $R = 40$. The general features of all these solutions and their development with Reynolds number are in agreement with experimental observations. For example, they indicate an approximately linear growth with Reynolds number of the standing vortex pair behind the cylinder. This is in agreement with the experiments of Taneda (1956).

On the other hand, solutions given by Allen & Southwell (1955) over the range $R = 0$ to 10^3 and by Dennis & Shimsoni (1965) for the range $R = 0{\cdot}01$ to 10^6 are generally thought to be unreliable at the higher Reynolds numbers. The main reason is that both sets of results indicate that the length of the vortex wake starts to decrease for some value of the Reynolds number between 10 and 100. This effect is most likely to be the result of numerical inaccuracy. Recent calculations by Hameliec & Raal (1969) also indicate an ultimate decrease in wake length as R increases. The only reliable solutions of the equations of steady motion beyond $R = 40$ appear to be the results of Takami & Keller (1969), in

which the Reynolds number range of calculations by Keller & Takami (1966, p. 115) has been extended to $R = 60$. These results again indicate linear dependence of wake length on Reynolds number up to $R = 60$. One of the main objectives of the present work has been to obtain some check on these results and to extend the Reynolds number range. It was found that reliable results could be obtained up to $R = 100$.

The second class of numerical solutions comes from integrating the time-dependent equations of motion. The first solutions for a circular cylinder were given by Payne (1958) for $R = 40$ and 100 and subsequently re-investigated by Ingham (1968), but Kawaguti & Jain (1966) appear to have been the first to have continued the integrations for sufficiently large times for a steady flow configuration to be reached. Steady solutions were obtained in this way for $R = 10$ up to 50, but solutions for $R = 60$ and 100 were discontinued after a large time and before a steady state was reached. The slow rate of approach to the final solution for larger values of the Reynolds number seems to be one of the main objections to obtaining steady solutions by integrating the time-dependent equations. Recent results of Son & Hanratty (1969) at $R = 40$, 200 and 500 seem to suggest that the wake in the cases $R = 200$, 500 had far from settled down when the integrations were stopped. The steady drag value at $R = 500$ was estimated by extrapolation.

Kawaguti & Jain had previously found it necessary to estimate steady drag values by extrapolation at higher Reynolds numbers. The same slow approach to the steady solution was noted when the present solutions were first attempted by time-dependent methods. Integrations at $R = 70$ and 100 were discontinued after a large time because of the extremely slow build up of the wake. It might also be noted th at solutions of the equations of steady motion may not be stable for these Reynolds numbers (see, for example, Van Dyke 1964, p. 150), and instability could tend to obviate an approach to the steady solution through the time-dependent problem. In any case, the general evidence seems to suggest that the. time-dependent method is not an efficient method of calculating steady solution s Its main use remains as a method of predicting flows which do not tend to a steady state as time increases. Solutions with this principal objective have been obtained by Hirota & Miyakoda (1965) and by Thoman & Szewczyk (1966).

One of the objects of obtaining numerical solutions for steady flow past a cylinder is to attempt to gain information on the nature of the theoretical steady flow limit as $R \to \infty$. This is still unknown, but various models have been suggested. A recent review by Roshko (1967) indicates concepts of considerably differing nature. The classical model is the discontinuous potential flow theory of Kirchhoff as propounded, for example, by Squire (1934) and Kawaguti (1953*a*). This model gives a finite drag on the cylinder as $R \to \infty$, with a wake of infinite length and zero velocity separated from an inviscid region by free streamlines. Batchelor (1956) has proposed a limiting solution with a closed wake of finite length, containing two regions with uniform vorticity, associated with zero drag on the body. Acrivos, Snowden, Grove & Petersen (1965) have suggested that the wake remains viscous in character as $R \to \infty$, and that its length grows linearly with the Reynolds number. This model is based mainly on the results of

experiments in which the wake was stabilized using a splitter plate, thereby allowing steady flow patterns to be obtained for Reynolds numbers up to 180. Further results in support of the model have been given by Acrivos, Leal, Snowden & Pan (1968).

In the present paper, the results of calculations for $R = 5, 7, 10, 20, 40, 70$ and 100 are given. They were obtained by solving finite-difference approximations to the equations of steady motion. Reasonable precautions have been taken to ensure that the solutions are accurate. The numerical procedures have been described fully by Dennis & Chang (1969*a*, 1969*b*) and will only be summarized. The results up to $R = 40$ are given in order to show the consistent development of the physical properties with Reynolds number. They are in excellent agreement with the results of Takami & Keller, and the numerical procedures are sufficiently different to provide a completely independent check. The development beyond $R = 40$ is also consistent with Takami & Keller's solutions and to some extent with the model of Acrivos *et al.*, in that the length of the wake continues to elongate in proportion to the Reynolds number and its breadth remains roughly of the order of the cylinder diameter.

2. Equations and method of approximation

The equations are given in dimensionless form, corresponding to a cylinder of radius $r = 1$ in a uniform stream of unit magnitude with its direction that of the positive axis of x. Modified polar co-ordinates (ξ, θ) are used, ξ where $= \log r$. The equations governing steady motion are:

$$\frac{\partial^2\zeta}{\partial\xi^2}+\frac{\partial^2\zeta}{\partial\theta^2} = \frac{R}{2}\left(\frac{\partial\psi}{\partial\theta}\frac{\partial\zeta}{\partial\xi}-\frac{\partial\psi}{\partial\xi}\frac{\partial\zeta}{\partial\theta}\right), \tag{1}$$

$$\frac{\partial^2\psi}{\partial\xi^2}+\frac{\partial^2\psi}{\partial\theta^2} = e^{2\xi}\zeta. \tag{2}$$

Here, ψ is the dimensionless stream function and ζ is the negative dimensionless vorticity. They are defined respectively by the equations $\psi = \psi'/Ua$ and $\zeta = -a\zeta'/U$, where ψ' and ζ' are the dimensional stream function and vorticity for a cylinder of radius a in a uniform stream U. The Reynolds number is defined in the usual way as $R = 2aU/\nu$. The flow is assumed to possess symmetry about the axis of x, and the boundary conditions necessary to obtain a solution in the region $\xi \geqslant 0$, $0 \leqslant \theta \leqslant \pi$ are

$$\psi = \frac{\partial\psi}{\partial\xi} = 0 \quad \text{for} \quad \xi = 0, \tag{3}$$

$$e^{-\xi}\frac{\partial\psi}{\partial\xi} \to \sin\theta, \quad e^{-\xi}\frac{\partial\psi}{\partial\theta} \to \cos\theta \quad \text{as} \quad \xi \to \infty, \tag{4}$$

$$\zeta \to 0 \quad \text{as} \quad \xi \to \infty, \tag{5}$$

$$\psi = \zeta = 0 \quad \text{for} \quad \theta = 0, \pi. \tag{6}$$

A numerical solution is obtained on the square grid shown in figure 1, which also shows the numbering system adopted for a set of points surrounding a

typical point 0. The line $\xi = \xi_m$ is taken as an outer boundary on which approximations to the conditions at infinity, equations (4) and (5), may be assumed to hold. The numerical method consists of replacing (1) by finite-difference approximations on this grid. It is convenient to write

$$\lambda(\xi, \theta) = -\tfrac{1}{4}R\frac{\partial \psi}{\partial \theta}, \quad \mu(\xi, \theta) = \tfrac{1}{4}R\frac{\partial \psi}{\partial \xi}. \tag{7}$$

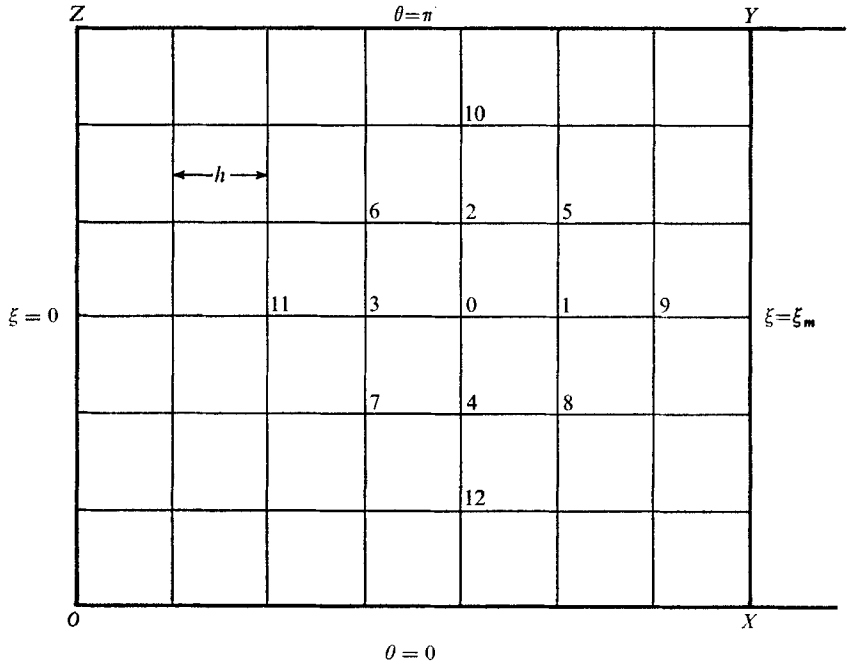

FIGURE 1. Domain of integration and grid structure.

The finite-difference equation obtained by replacing derivatives in (1) by the simplest possible approximations in central differences at 0 is

$$(1+h\lambda_0)\zeta_1+(1+h\mu_0)\zeta_2+(1-h\lambda_0)\zeta_3+(1-h\mu_0)\zeta_4-4\zeta_0 = 0. \tag{8}$$

Satisfaction of (8) at every internal grid point of the region $OXYZ$ of figure 1, subject to boundary conditions for ζ at every grid point of the boundary $OXYZ$, defines a numerical approximation to the solution of (1).

Boundary conditions on OX and YZ are given by (6), and we can take $\zeta = 0$ on XY as a crude approximation to (5), assuming ξ_m large enough. An improvement on this latter boundary condition is given by Dennis & Chang (1969*a*). The approximation $\zeta = 0$ is replaced by, effectively, a gradient condition for ζ, on the assumption that the flow for $\xi \geqslant \xi_m$ is governed by Oseen's linearized equations. The details are almost the same as those already published by Dennis, Hudson & Smith (1968) and will be mentioned only briefly. The Oseen problem, which is valid for large ξ, is obtained by replacing the derivatives of ψ in (1) by the expressions obtained from the boundary conditions (4). The equation which

results can then be solved formally and from the solution it is deduced, provided ξ is large enough, that

$$\zeta(\xi, \theta) \sim G(\theta)\, \chi^{-\frac{1}{2}} \exp\{\chi(\cos\theta - 1)\}, \tag{9}$$

where $\chi = \frac{1}{4}R\, e^{\xi}$. Here, $G(\theta)$ is a function of θ alone and thus, if (9) is assumed to hold for $\xi \geqslant \xi_m$, we obtain the approximation

$$\zeta(\xi, \theta) = \zeta(\xi_m, \theta) \exp\{(\chi - \chi_m)(\cos\theta - 1) - \tfrac{1}{2}(\xi - \xi_m)\}, \tag{10}$$

where χ_m is the value of χ at $\xi = \xi_m$. In particular, if we put $\xi = \xi_m + h$ in (10), an expression for $\zeta(\xi_m + h, \theta)$ in terms of $\zeta(\xi_m, \theta)$ is obtained which can be used, in a similar manner to a gradient-type boundary condition, to eliminate ζ_1 from (8) whenever the point 0 is situated on $\xi = \xi_m$.

The condition for ζ on $\xi = 0$ depends upon the solution of (2). It is in the method of solution of (2) and the calculation of boundary values of ζ on $\xi = 0$ that the present method differs from the usual finite-difference procedure. A solution of (2) is assumed in the form

$$\psi(\xi, \theta) = \sum_{n=1}^{\infty} f_n(\xi) \sin n\theta, \tag{11}$$

which automatically satisfies the conditions for ψ in (6). Substitution in (2) gives

$$f_n'' - n^2 f_n = r_n(\xi) \quad (n = 1, 2, 3, \ldots). \tag{12}$$

Here, primes denote differentiation with regard to ξ and

$$r_n(\xi) = \frac{2e^{2\xi}}{\pi} \int_0^{\pi} \zeta \sin n\theta \, d\theta. \tag{13}$$

From (3) it follows that

$$f_n(0) = f_n'(0) = 0, \tag{14}$$

and the equations (12) can be solved as a step-by-step integration, provided $r_n(\xi)$ is known for sufficient values of n (say up to n_0) on all grid lines of constant ξ from $\xi = 0$ to $\xi = \xi_m$. The number n_0 is the number of terms taken to approximate the infinite sum in (11). One further equation is necessary to complete the procedure. It can be deduced from the properties of the solutions of (12). In order that (4) shall be satisfied it is necessary that the condition

$$\int_0^{\infty} e^{-n\xi} r_n(\xi) \, d\xi = 2\delta_n \tag{15}$$

is satisfied, where $\delta_1 = 1$ and $\delta_n = 0$ $(n = 2, 3, \ldots)$. When the left side of (15) is expressed as a numerical quadrature formula over the grid lines of constant ξ, and with the upper limit approximated by ξ_m, it gives a formula for $r_n(0)$ in terms of grid values of $r_n(\xi)$ for $\xi \neq 0$. Thus, the condition (15) is used for calculating values of $r_n(0)$. From these values we can calculate $\zeta(0, \theta)$ from the result

$$\zeta(\xi, \theta) = e^{-2\xi} \sum_{n=1}^{\infty} r_n(\xi) \sin n\theta, \tag{16}$$

which follows from (13). In practice, the summation is again approximated by n_0 terms.

3. Calculation procedure

Suppose that a grid size h, a value for ξ_m, and a value for n_0 have been assigned for a given Reynolds number. A numerical solution is obtained by repeating the following cycle of steps until convergence is achieved. Suppose a starting approximation to ψ is known and a boundary condition $\zeta(0,\theta)$ has been calculated from (16), using values of $r_n(0)$ determined to satisfy (15). Then:

(i) $\zeta(\xi,\theta)$ is determined by solving the equations (8) subject to the calculated boundary condition for $\zeta(0,\theta)$ and the other specified conditions on the remaining boundaries.

(ii) $r_n(\xi)$, $(n = 1, 2, \ldots, n_0)$ is calculated from (13) for all $\xi \neq 0$.

(iii) $r_n(0)$ is calculated to satisfy (15) and hence a new approximation to $\zeta(0,\theta)$ is found from (16).

(iv) The equations (12) are solved for $n = 1, 2, \ldots, n_0$ and a new approximation to $\psi(\xi,\theta)$ found from (11). This completes one cycle of the iteration.

Convergence of the procedure is decided by comparing some representative feature of two successive solutions. Many comparisons are possible. The one chosen was

$$|r_n^{(m+1)}(0) - r_n^{(m)}(0)| < \epsilon$$

for all $n \leqslant n_0$, where ϵ is a specified accuracy parameter and m, $m+1$ denote two successive iterates. This is a very representative convergence test because each $r_n(0)$, through (13) and then through (15), is calculated from a weighted sum involving every value of ζ (except those on $\xi = 0$) in the computational field. The test ensures, through (16), that the boundary vorticity has converged. One of the interesting features of the present method is that the vorticity on the cylinder is calculated by integration right throughout the field rather than from a few isolated values of ψ near $\xi = 0$, as is the case in the usual finite-difference method of approximating (2). Moreover, equation (16) determines $\zeta(0,\theta)$ as a continuous function of θ more or less regardless of the grid size used in solving (1) provided, of course, that it is reasonably small. Features of the flow at the cylinder surface, such as the point of separation of the flow, can be determined accurately from (16).

The calculation procedure has been described in more detail by Dennis & Chang (1969*a*, 1969*b*) and only two points will be mentioned. The numerical evaluation of $r_n(\xi)$ from (13) is performed using the method of Filon (1928), since this gives uniformly accurate results, even if n is large. Finally, at stage (iii) of the above calculation procedure, the new value of $\zeta(0,\theta)$ is not introduced directly as a new boundary condition on OZ. If a previous boundary condition $\zeta^{(m)}(0,\theta)$ gives rise, at stage (iii), to a calculated value $\zeta^*(0,\theta)$, the actual value introduced in the next iteration is

$$\zeta^{(m+1)}(0,\theta) = \kappa\zeta^*(0,\theta) + (1-\kappa)\,\zeta^{(m)}(0,\theta),$$

where $0 < \kappa \leqslant 1$. This is an empirical process of averaging which may prevent divergence of the iterations, by taking κ small enough. It has been used in a number of the numerical studies cited in the introduction, often in a wider context than that used here, where it is applied only to the boundary of the cylinder.

Numerical solutions have been obtained for values of the parameters shown in table 1. The values of κ could possibly be considerably larger; this point has not been fully investigated. For each Reynolds number, a numerical solution was obtained, using the above iterative method, in which the approximation to $\zeta(\xi, \theta)$ ultimately satisfied (8). Then, in order to check the accuracy and improve

R	h	ξ_m/π	n_0	κ
5	$\pi/40$	1	20	0·05
7	$\pi/40$	1	20	0·05
10	$\pi/40$	1	20	0·05
20	$\pi/40$	1	30	0·05
40	$\pi/40$	1	30	0·05
70	$\pi/60$	7/6	40	0·03
100	$\pi/60$	7/6	40	0·015

TABLE 1. Parameters used in the calculations

upon it, the difference correction method of Fox (1947) was used to obtain a higher approximation to (1). If L_0 denotes the left side of (8), a higher approximation to (1) which takes into account all central differences up to the fifth can be written

$$L_0 + K_0 = 0, \tag{17}$$

where

$$12K_0 = 4(1+h\lambda_0)\zeta_1 + 4(1+h\mu_0)\zeta_2 + 4(1-h\lambda_0)\zeta_3 + 4(1-h\mu_0)\zeta_4 - (1+2h\lambda_0)\zeta_9 - (1+2h\mu_0)\zeta_{10} - (1-2h\lambda_0)\zeta_{11} - (1-2h\mu_0)\zeta_{12} - 12\zeta_0. \tag{18}$$

When the grid size is small enough, the correction K_0, evaluated using the converged solution which satisfies $L_0 = 0$, should be reasonably small everywhere. This gives some check that the grid size has been chosen properly.

An improvement to the solution can be obtained by setting up a new iteration which includes the correction. If in the old iteration, without correction, an iterate $\zeta^{(m)}(\xi, \theta)$ is obtained by solving the difference equations $L_0^{(m)} = 0$, the new iteration consists of solving the equations

$$L_0^{(m)} + K_0^{(m-1)} = 0. \tag{19}$$

Here, the vector K_0 is calculated from the previous iterate $\zeta^{(m-1)}(\xi, \theta)$ and held fixed during the determination of the new iterate $\zeta^{(m)}(\xi, \theta)$. Provided the initial correction is small enough, the sequence of iterates converges to a limit which satisfies (17), in which L_0 and K_0 are mutually consistent.

There is no difficulty in calculating the correction K_0 at any point of the field. On grid lines adjacent to $\theta = 0$ and $\theta = \pi$, the formula (18) involves values of ζ which lie outside the field of computation $OXYZ$, but these can be expressed in terms of internal values of ζ from the relations

$$\zeta(\xi, -\theta) = -\zeta(\xi, \theta), \quad \zeta(\xi, \pi+\theta) = -\zeta(\xi, \pi-\theta),$$

which hold because the flow is symmetrical about the axis of x. External values of ζ also enter the calculation of K_0 at grid points on XY and on the adjacent

grid line $\xi = \xi_m - h$. In view of the fact that the boundary condition on $\xi = \xi_m$ rests on the assumption that the flow for $\xi \geqslant \xi_m$ is Oseen flow, the necessary external values are calculated from (10). Finally, if the typical point 0 is on the grid line $\xi = h$, the value ζ_{11} is external to the field. In this case

$$\partial^2\zeta/\partial\xi^2 + \partial^2\zeta/\partial\theta^2 = 0 \quad \text{when} \quad \xi = 0$$

and hence, approximately,

$$\zeta_{11} = 4\zeta_3 - \zeta_0 - \zeta_6 - \zeta_7,$$

which enables ζ_{11} to be calculated from internal and boundary values of ζ.

In the present results, the difference correction method yielded only a small change from the solutions computed to satisfy (8). For the lower Reynolds numbers the changes in the main physical properties, such as the total drag coefficient, were almost negligible while for $R = 70$ and 100 the properties changed by only a few per cent, certainly less than 5 %. This suggests that the final results are of good accuracy, and also that the grid sizes given in table 1 are satisfactory. The values of ξ_m in table 1 which give the position of the outer boundary XY were obtained as the result of experience, as also was the number of terms, n_0, used to approximate the infinite sums on the right sides of (11) and (16). The effect of varying both of these parameters was studied, and it was found that an increase in either parameter beyond the values indicated in the table had negligible effect on the computed solution. The whole question of the effect of the imposed boundary conditions on $\xi = \xi_m$ on the internal solution has been discussed in detail by Dennis & Chang (1969*a*).

4. Results

Streamlines of the motion for the range $R = 5$–100 are shown in figure 2. Separation has started at $R = 7$, and the length of the wake, L, from the rear of the cylinder to the end of the separated region, grows approximately linearly with R over the whole range. The calculated length of the wake is compared with other theoretical calculations and with experimental measurements in figure 3. It is also given numerically in table 2. There is very good agreement with the recent calculations of Takami & Keller up to $R = 60$, and the same straight-line development is continued beyond this by the present results. Kawaguti & Jain's results, obtained by time-dependent methods, appear to be departing from the linear relationship after $R = 20$. Son & Hanratty do not give the steady wake length for Reynolds numbers greater than 40.

Despite good agreement of Kawaguti & Jain with Son & Hanratty for the wake length of about $L = 5$ at $R = 40$, both investigations have used the rather coarse grid size $\pi/30$ in the θ direction. This may lead to a spurious lengthening of the wake, for a similar effect was observed in an attempt, by present methods, to obtain the time-dependent flow at $R = 100$ with a square grid of size $\pi/40$. By the time L had reached its steady limit it was almost 22, nearly 11 diameters of the cylinder. The vortex pair had also become distorted and fat, very much after the manner of Son & Hanratty's results for $R = 200$ and 500. A reduction

of the grid size to $\pi/60$ gave, in essence, the results of figure 2(*g*), although it was not possible to continue the integrations to the fully steady state. Although Son & Hanratty have used a rectangular grid, with considerably smaller grid sizes in the ξ direction, the grid size in the θ direction is rather coarse. In the wake at large distances, the grid size in the θ direction dominates the accuracy at least as much as that in the ξ direction. This is evident from the rapid exponential

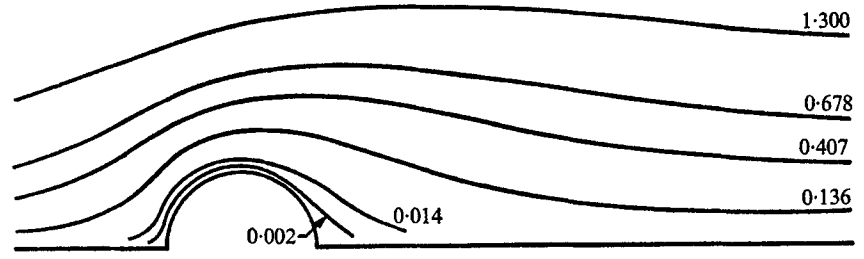

(*a*)

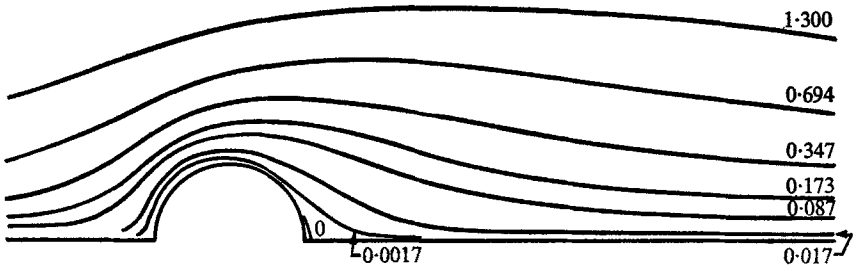

(*b*)

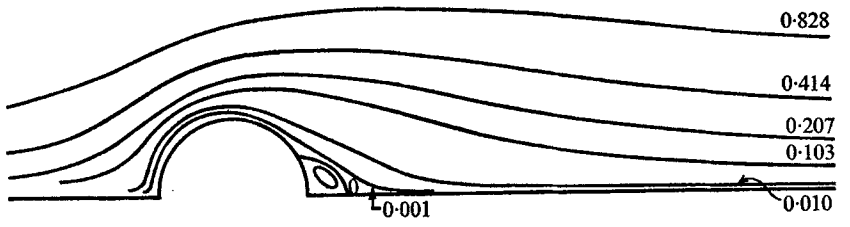

(*c*)

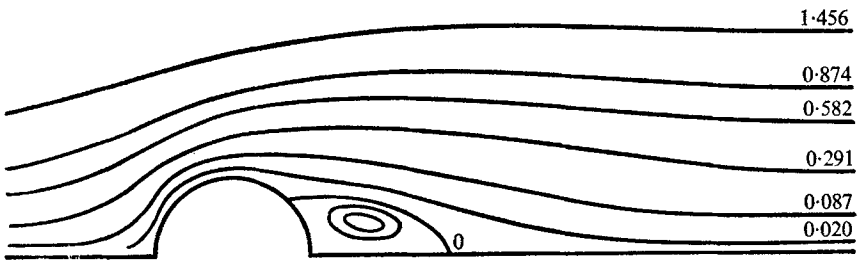

(*d*)

FIGURES 2(*a–d*). For legend see p. 480.

variation of ζ in the θ direction when ξ is large, as indicated by the expression (9) obtained from Oseen theory. The variation depends, essentially, on how rapidly $\chi(1-\cos\theta)$ varies with θ for a given value of χ. The grid size in the θ direction should be small enough to allow representation of the exponential variation adequately by finite differences for the largest value of χ, $\chi = \chi_m$, in the domain of the numerical solution. This point has been considered more fully by Dennis & Chang (1969*a*).

The vorticity vanishes at the point of separation and it follows from (16) that the angle of separation, $\theta = \theta_s$, is a root of

$$\sum_{n=1}^{\infty} r_n(0) \sin n\theta = 0. \tag{20}$$

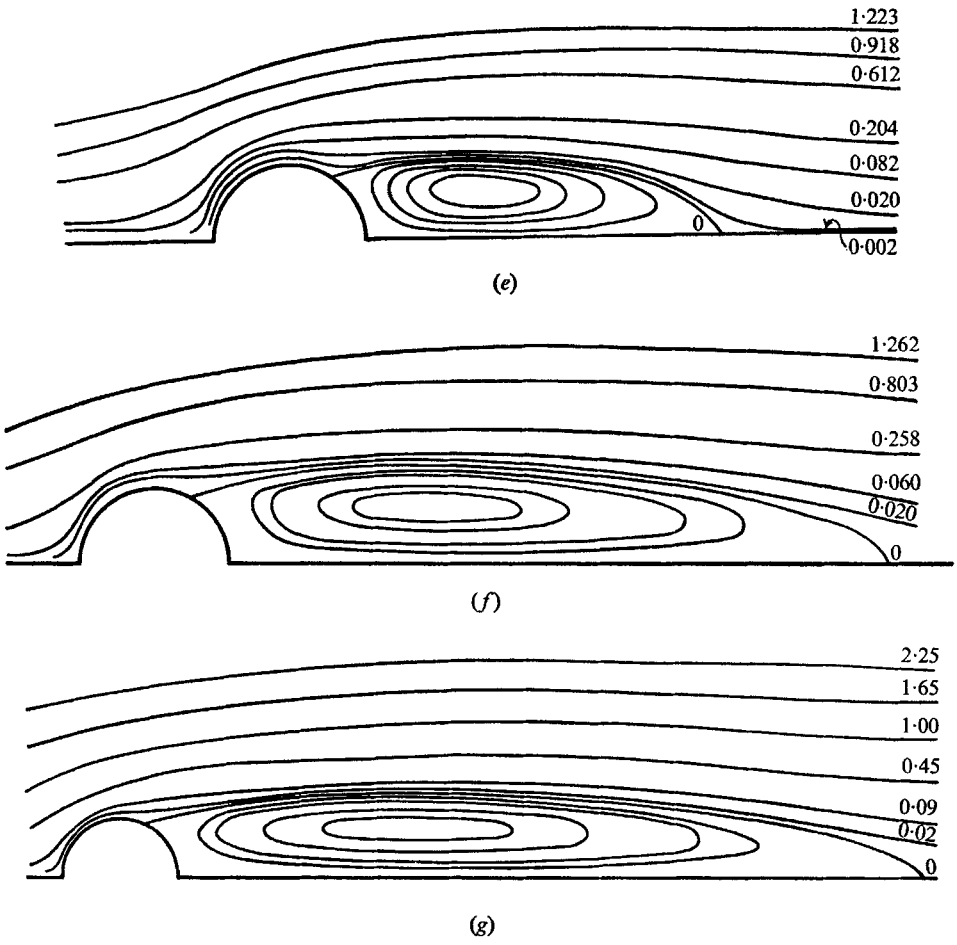

FIGURE 2. Streamlines for steady flow past a circular cylinder. Values of the dimensionless stream function, ψ, are shown for each streamline. Values of ψ for the closed streamlines, ψ_c, are given following the Reynolds number, where appropriate, starting from the centre of the wake. (*a*) $R = 5$; (*b*) $R = 7$; (*c*) $R = 10$: $\psi_c = -0{\cdot}0002$; (*d*) $R = 20$: $\psi_c = -0{\cdot}008$, $-0{\cdot}0058$; (*e*) $R = 40$: $\psi_c = -0{\cdot}0328$, $-0{\cdot}0246$, $-0{\cdot}0164$, $-0{\cdot}0082$; (*f*) $R = 70$: $\psi_c = -0{\cdot}07$, $-0{\cdot}06$, $-0{\cdot}035$, $-0{\cdot}023$; (*g*) $R = 100$: $\psi_c = -0{\cdot}1$, $-0{\cdot}08$, $-0{\cdot}05$, $-0{\cdot}035$.

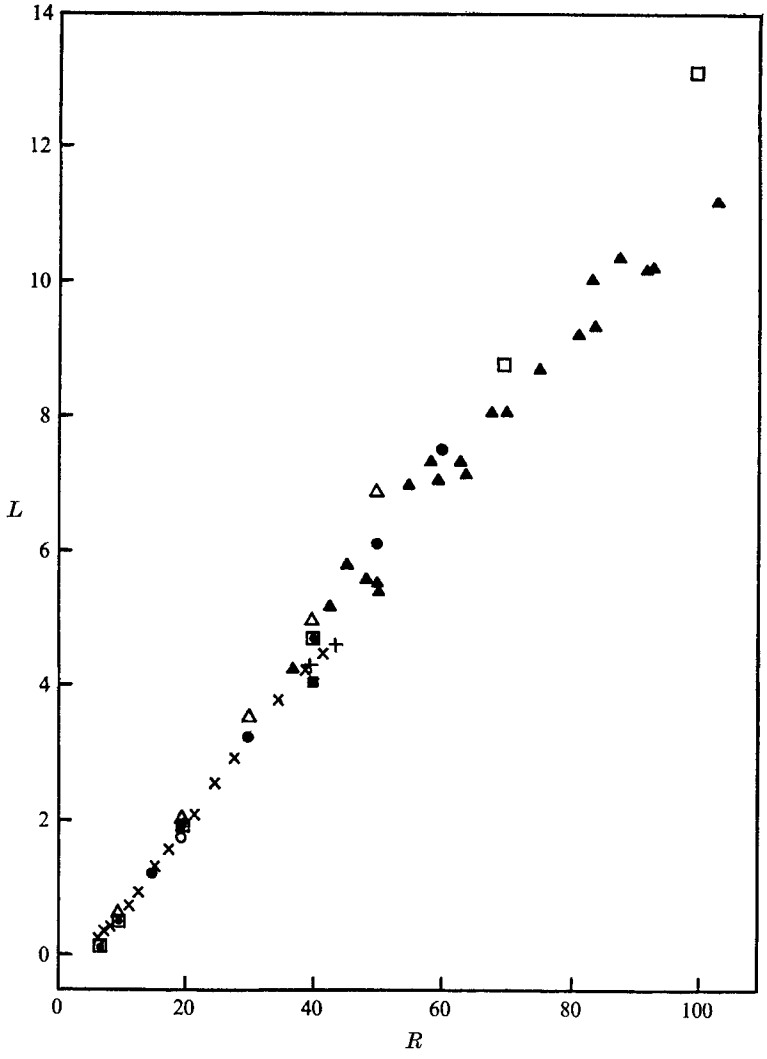

FIGURE 3. Calculated and experimental values for the wake length. Numerical solutions: □, this study; ●, Takami & Keller (1969); Δ, Kawaguti & Jain (1966); +, Apelt (1961); ■, Kawaguti (1953*b*); ○, Thom (1933). Experimental measurements: ▲, Acrivos *et al.* (1968): ×, Taneda (1956).

R	L	θ_s	C_f	C_p	C_D	$P(0)$	$P(\pi)$
5	—	—	1·917	2·199	4·116	−1·044	1·872
7	0·19	15·9	1·553	1·868	3·421	−0·870	1·660
10	0·53	29·6	1·246	1·600	2·846	−0·742	1·489
20	1·88	43·7	0·812	1·233	2·045	−0·589	1·269
40	4·69	53·8	0·524	0·998	1·522	−0·509	1·144
70	8·67	61·3	0·360	0·852	1·212	−0·439	1·085
100	13·11	66·2	0·282	0·774	1·056	−0·393	1·060

TABLE 2. Calculated properties of the numerical solutions. The angle of separation, θ_s, is given in degrees

Calculated values of θ_s are given in table 2. They are in extremely good agreement with the calculations of Takami & Keller, who give the respective values $\theta_s = 14{\cdot}5°$, $29{\cdot}3°$, $43{\cdot}65°$, $53{\cdot}55°$, $56{\cdot}6°$, $59{\cdot}0°$ at the Reynolds numbers 7, 10, 20, 40, 50 and 60. Son & Hanratty's value at $R = 40$ is $\theta_s = 53{\cdot}9°$, while Kawaguti & Jain's is $53{\cdot}7°$. Separation first starts to take place at some critical Reynolds number between 5 and 7 for which $\theta_s = 0$. It may be deduced with the aid of (16) that this Reynolds number is that which makes the sum

$$B(R) = \sum_{n=1}^{\infty} n r_n(0)$$

vanish. The approximations $B(5) = 0{\cdot}100$ and $B(7) = -0{\cdot}068$ are obtained from the present results. A linear interpolation suggests the critical Reynolds number as $R = 6{\cdot}2$.

The dimensionless drag coefficient is defined by $C_D = D/\rho U^2 a$, where D is the total drag on the cylinder, and ρ is the density. The total drag may be obtained by integrating the total stress component in the direction of x around the surface of the cylinder. If p is the pressure and, as previously noted, ζ' is the dimensional scalar vorticity, then

$$D = -\int_0^{2\pi} (\rho\nu\zeta'_0 \sin\theta + p_0 \cos\theta)\, a\, d\theta,$$

where ν is the coefficient of kinematical viscosity and the subscript zero denotes a value at $\xi = 0$. The second term in the integral may be dealt with conveniently by integrating by parts and eliminating the pressure gradient using the equation of motion in the direction of θ. It may then be shown that

$$C_D = \frac{4}{R}\int_0^{\pi} \zeta_0 \sin\theta\, d\theta - \frac{4}{R}\int_0^{\pi} (\partial\zeta/\partial\xi)_0 \sin\theta\, d\theta. \tag{21}$$

The first term on the right gives the friction drag coefficient and the second the pressure drag coefficient, denoted respectively by C_f and C_p. If the result (16) is substituted, the simple expressions

$$C_f = 2\pi r_1(0)/R,$$

$$C_p = 2\pi\{2r_1(0) - r'_1(0)\}/R$$

are obtained, where the prime denotes differentiation with regard to ξ. Actually, it was found to be slightly more satisfactory to calculate C_p by direct numerical evaluation of the second integral in (21) using values of $(\partial\zeta/\partial\xi)_0$ obtained by numerical differentiation. Calculated drag coefficients are given in table 2 and also in figure 4, where the total drag coefficient is compared with other numerical results obtained from integrations of the equations of steady motion and with the experimental measurements of Tritton (1959). A recent estimate of $C_D = 1{\cdot}172$ at $R = 100$ has been given by Hameliec & Raal, but the associated wake length of $L = 9{\cdot}48$ seems much too low and is likely to be due to the fact that the boundary $\xi = \xi_m$ has been taken too close to the cylinder.

The drag coefficient calculated from (21) enables some check to be made on the corresponding numerical solution in view of the fact that the nature of the

flow at large distances is known. From the solution of Imai (1951) it is known that, as $\xi \to \infty$,

$$\psi(\xi, \theta) \sim e^{\xi} \sin\theta - \tfrac{1}{2} C_D (1 - \theta/\pi),$$

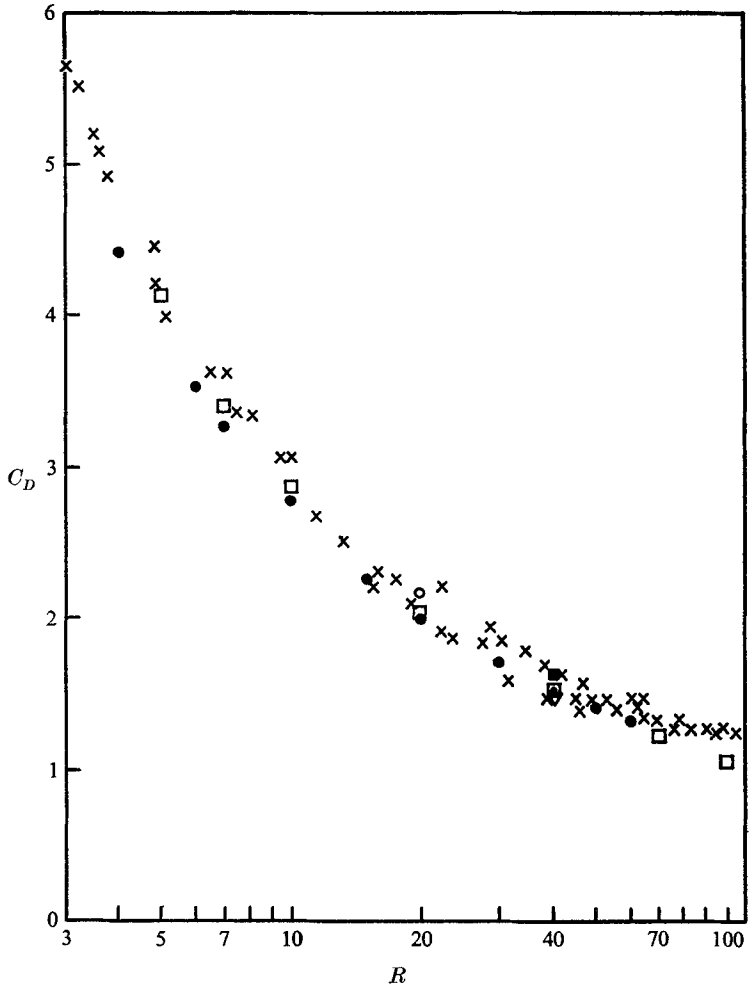

FIGURE 4. Calculated and experimental values for the total drag coefficient. Numerical solutions of the equations of steady motion: □, this study; ●, Takami & Keller (1969); ▽, Apelt (1961); ■, Kawaguti (1953*b*); ○, Thom (1933). Experimental measurements: ×, Tritton (1959).

except on $\theta = 0$, where a finite discontinuity exists. It follows that the solution of the set of equations (12) must be such that

$$f_n(\xi) \sim \delta_n e^{\xi} - C_D/\pi n, \tag{22}$$

where δ_n has the meaning already assigned in (15). In the numerical procedure, the coefficient of $1/n$ on the right side of (22) is not specified, but emerges as the result of the calculations. This gives the required check, although it is a stringent one and cannot be expected to be satisfied to high precision, since, effectively,

it checks the balance of outflow and inflow over a very large contour surrounding the cylinder. It may be applied to the numerical solutions, for example, by subtracting the exponential term from the right side of (22) when $n = 1$ and comparing the tendency of the remainder, as ξ increases, with the value obtained using (21).

In all the computed results, a tendency consistent with (22) was observed, but the precision of the check is hindered by two factors. First, it is not known how closely the limiting behaviour should be approached at the finite upper limit, $\xi = \xi_m$, imposed on a given numerical solution. Further, any attempt to increase ξ_m unduly leads to a fluctuation in the coefficient of $1/n$ in (22) as calculated by the numerical integration procedure. This is noticeable only near $\xi = \xi_m$ and is due to the increasingly poor finite-difference approximation to ζ in the wake. On the whole, however, the coefficient of $1/n$ as determined from the numerical integration was found to approach within about 10 % of the theoretical value consistent with calculation from (21), which is considered to be satisfactory in view of the two factors mentioned. Some other numerical checks were also carried out. For example, the effect of varying the number, n_0, of terms used to approximate the summation on the right side of (11) was considered. More terms are needed as R is increased, but $n_0 = 40$ is still adequate at $R = 100$. If we take, as an illustration, the variation of wake length with n_0 at this Reynolds number we find $L = 9{\cdot}12$, $12{\cdot}03$ and $12{\cdot}99$ at values $n_0 = 10$, 20, 30. The final value (table 2) for $n_0 = 40$ is $L = 13{\cdot}1$.

One of the possible models for the limiting flow as $R \to \infty$ is the discontinuous potential flow of Kirchhoff type. Imai (1957) has given the large Reynolds number formula

$$C_D^{\frac{1}{2}} \sim C_{D\infty}^{\frac{1}{2}} + \alpha R^{-\frac{1}{2}} \tag{23}$$

based on this model. Here, α is an unknown constant and $C_{D\infty}$ is the drag coefficient of the limiting Kirchhoff flow. Brodetsky (1923) gives $C_{D\infty} = 0{\cdot}5$ for a circular cylinder. On the basis of this value, Takami & Keller have estimated α by evaluating it from (23) using their drag values at $R = 50$ and 60, and then extrapolating linearly in R^{-1} as $R \to \infty$. The value obtained in this way is $\alpha = 3{\cdot}547$. A similar procedure carried out with the present values of C_D at $R = 70$ and 100 gives $\alpha = 2{\cdot}99$. This discrepancy in estimates of α is a little too large to assume any reliable confirmation of the formula (23), and neither value of α gives values of C_D which compare particularly well with the calculated values $C_D = 0{\cdot}924$ and $0{\cdot}60$ given by Son & Hanratty at $R = 200$ and 500. On the other hand, if we assume an asymptotic boundary-layer-type expansion for the friction drag in powers of $R^{-\frac{1}{2}}$, and fit the first two terms to the present results for $R = 70$ and 100, we obtain

$$C_f \sim 1{\cdot}83R^{-\frac{1}{2}} + 9{\cdot}95R^{-1}.$$

This not only fits the value at $R = 40$, but gives respective values $C_f = 0{\cdot}18$ and $0{\cdot}10$ at $R = 200$ and 500. These compare well with Son & Hanratty's respective values $C_f = 0{\cdot}19$ and $0{\cdot}09$.

The dimensionless pressure coefficient

$$P(\theta) = \frac{p_0(\theta) - p_\infty}{\frac{1}{2}\rho U^2}, \tag{24}$$

where $p_0(\theta)$ is the pressure on the cylinder surface and p_∞ the uniform pressure at large distances, is calculated from the formula

$$P(\theta) = 1 - \frac{4}{R}\int_0^\infty \left(\frac{\partial\zeta}{\partial\theta}\right)_{\theta=\pi} d\xi + \frac{4}{R}\int_\theta^\pi \left(\frac{\partial\zeta}{\partial\xi}\right)_{\xi=0} d\theta. \tag{25}$$

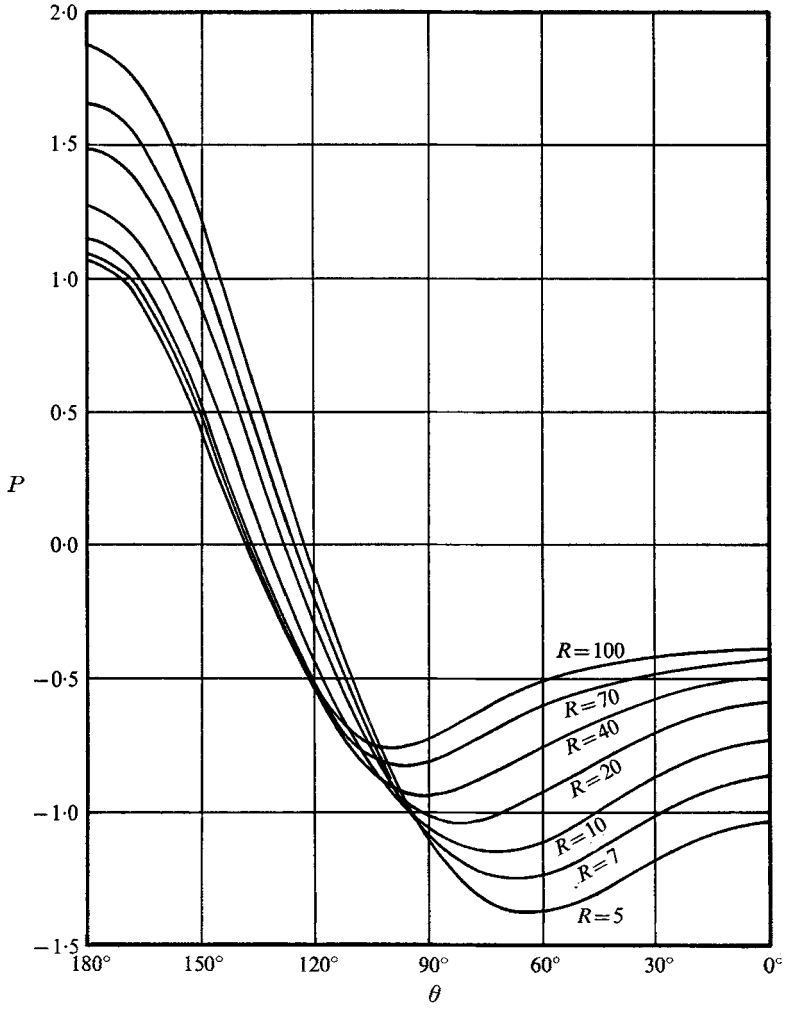

FIGURE 5. Pressure coefficient on the cylinder surface.

Curves of the pressure coefficient are given in figure 5, and its values at the rear and the front of the cylinder are given in table 2. Both of these values are of interest. According to the exact solution for stagnation point flow (see Schlichting 1960), the coefficient at the front of the cylinder should behave, for large Reynolds number, like

$$P(\pi) \sim 1 + \beta R^{-1}, \tag{26}$$

where β is a constant. Takami & Keller have estimated $\beta = 5{\cdot}985$ by calculation from (26) at $R = 50$ and 60, followed by linear extrapolation in R^{-1} as $R \to \infty$.

A similar extrapolation from the present results at $R = 70$ and 100 gives $\beta = 6{\cdot}09$, which is in reasonable agreement.

The variation with R of the pressure coefficient at the rear of the cylinder is of interest in view of two models which have been proposed for the separated flow at high Reynolds number. In a model suggested by Roshko and by Sychev (1967), the behaviour for large Reynolds numbers should be

$$P(0) \sim AR^{-\frac{1}{2}}, \tag{27}$$

where A is a constant. The model of Acrivos *et al.* (1965) suggests that $P(0)$ becomes constant as the Reynolds number increases. Recent experimental observations of Acrivos *et al.* (1968) tend to confirm this. It is found that the

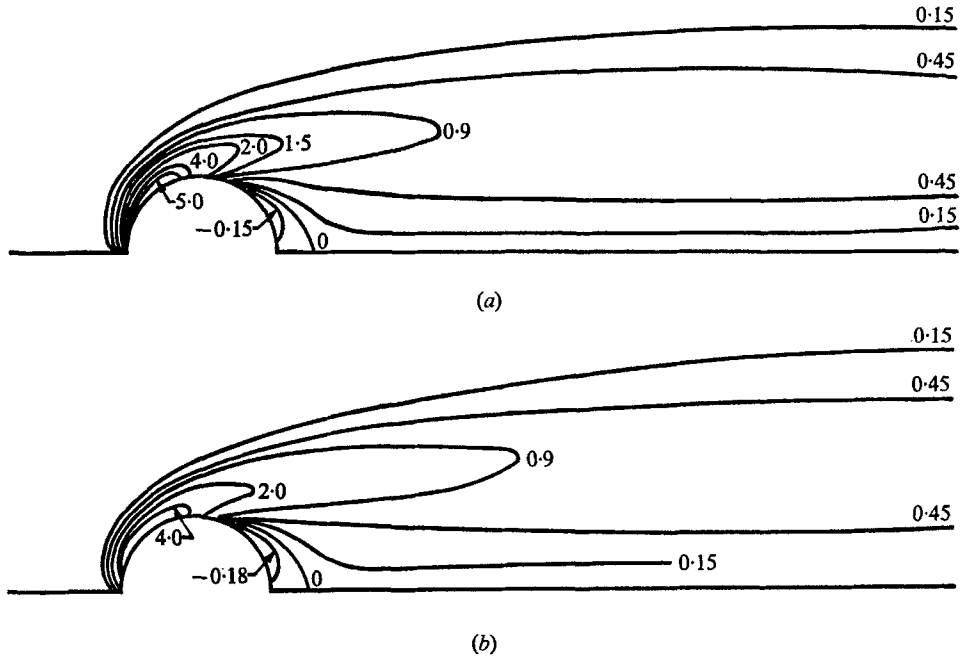

FIGURE 6. Equi-vorticity lines for steady flow past a circular cylinder. Values of the negative dimensionless vorticity, ζ, are shown for each equi-vorticity line. (*a*) $R = 70$; (*b*) $R = 100$.

observed coefficient tends to become constant at quite moderate values of R, of the order of 100. Unfortunately, the results of the present calculations do not give any definite information one way or the other. The variation of $P(0)$ is not rapid enough to fit (27). Neither is this coefficient obviously approaching a constant, at least, certainly not in the range $-0{\cdot}47$ to $-0{\cdot}43$ suggested by the experimental results for circular cylinders. This point requires further elucidation.

The variation of vorticity throughout the flow field for Reynolds numbers 70 and 100 is indicated by equi-vorticity lines in figure 6. For lower Reynolds numbers, the vorticity distributions are, in essence, the same as those given by Takami & Keller. The dimensionless negative vorticity on the surface of the cylinder is shown in figure 7. No reasonable prediction can be made as to its

tendency for large Reynolds number and, in particular, as to the ultimate position of the separation point. Son & Hanratty have noted that in their solutions for late times, the vorticity near the front stagnation point is significantly less than that predicted by boundary-layer theory with the potential solution for the

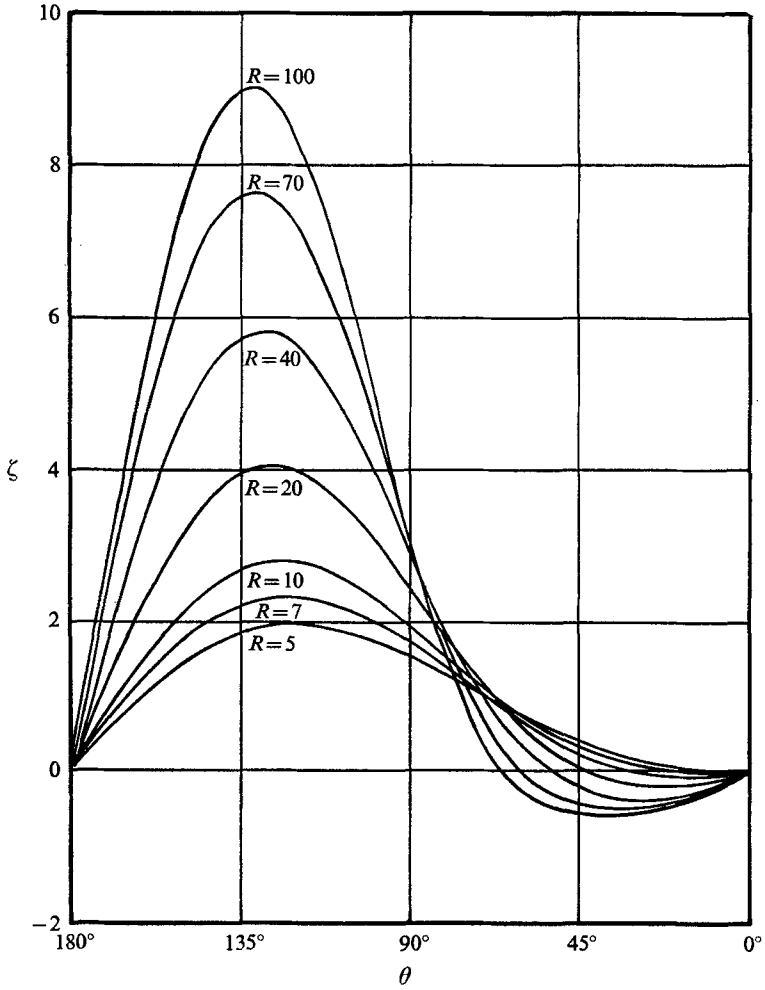

FIGURE 7. Vorticity distribution over the surface of the cylinder.

external flow. The same effect has been noted in the present solutions and may be indicated as follows. The local coefficient of skin friction is $c_f = \tau_0/\frac{1}{2}\rho U^2$, where τ_0 is the local shearing stress, and it follows that

$$c_f = 4R^{-1}\zeta(0, \theta).$$

In the neighbourhood of the front stagnation point we put $\theta = \pi - \phi$, and it may then be deduced from (16) that, for small ϕ,

$$R^{\frac{1}{2}}c_f \sim S\phi, \tag{28}$$

where

$$S(R) = 4R^{-\frac{1}{2}} \sum_{n=1}^{\infty} (-1)^{n+1} n r_n(0).$$

As $R \to \infty$, $S(R)$ should tend to the constant value of approximately 9·861 consistent with stagnation point flow (Schlichting 1960, p. 153). For the three highest Reynolds numbers $R = 40$, 70 and 100, the series $S(R)$ converges rapidly, and we obtain the respective values

$$S(R) = 6{\cdot}59,\ 6{\cdot}70,\ 6{\cdot}89.$$

The discrepancy with boundary-layer flow at these Reynolds numbers is therefore substantial.

Part of the work described in this paper was carried out while one author (S.C.R.D.) was a visitor to the Mathematics Research Centre, U.S. Army, University of Wisconsin. A detailed account of the investigation, including full details of the numerical method, is given in the report by Dennis & Chang (1969*a*) which has been cited. Copies of this report can be obtained from the Mathematics Research Centre, and a copy has been deposited in the editorial office of the Journal of Fluid Mechanics.

Part of the work was supported by Contract no. DA-31-124-ARO-D-462, and part was sponsored by the National Research Council of Canada. The numerical calculations were performed on the CDC 3600 of the University of Wisconsin and on the IBM 7040 of the University of Western Ontario.

REFERENCES

Acrivos, A., Leal, L. G., Snowden, D. D. & Pan, F. 1968 *J. Fluid Mech.* **34**, 25.

Acrivos, A., Snowden, D. D., Grove, A. S. & Petersen, E. E. 1965 *J. Fluid Mech.* **21**, 737.

Allen, D. N. De G. & Southwell, R. V. 1955 *Quart. J. Mech. Appl. Math.* **8**, 129.

Apelt, C. J. 1961 *Aero. Res. Counc. R. & M.* no. 3175.

Batchelor, G. K. 1956 *J. Fluid Mech.* **1**, 388.

Brodetsky, S. 1923 *Proc. Roy. Soc.* A **102**, 542.

Dennis, S. C. R. & Chang, G. Z. 1969*a* *Mathematics Research Centre, U.S. Army, Madison, Wisconsin, Technical Summary Report*, no. 859.

Dennis, S. C. R. & Chang, G. Z. 1969 *Phys. Fluids Suppl.* II, **12**, II–88.

Dennis, S. C. R., Hudson, J. D. & Smith, N. 1968 *Phys. Fluids*, **11**, 933.

Dennis, S. C. R. & Shimshoni, M. 1965 *Aero. Res. Counc. Current Paper*, no. 797.

Filon, L. N. G. 1928 *Proc. Roy. Soc. Edinb.* **49**, 38.

Fox, L. 1947 *Proc. Roy. Soc.* A **190**, 31.

Hamielec, A. E. & Raal, J. D. 1969 *Phys. Fluids*, **12**, 11.

Hirota, I. & Miyakoda, K. 1965 *J. Met. Soc. Japan*, Ser. II, **43**, 30.

Imai, I. 1951 *Proc. Roy. Soc.* A **208**, 487.

Imai, I. 1957 *University of Maryland Tech. Note*, no. BN-104.

Ingham, D. B. 1968 *J. Fluid Mech.* **31**, 815.

Kawaguti, M. 1953*a* *J. Phys. Soc. Japan*, **8**, 403.

Kawaguti, M. 1953*b* *J. Phys. Soc. Japan*, **8**, 747.

Kawaguti, M. & Jain, P. 1966 *J. Phys. Soc. Japan*, **21**, 2055.

Keller, H. B. & Takami, H. 1966 In *Numerical Solutions of Nonlinear Differential Equations*. (Ed. D. Greenspan.) Englewood Cliffs, N.J.: Prentice-Hall.

Payne, R. B. 1958 *J. Fluid Mech.* **4**, 81.

Roshko, A. 1967 *Proc. Canadian Congress of Applied Mechanics*, **3**, 81.

SCHLICHTING, H. 1960 *Boundary Layer Theory*. New York: McGraw-Hill.

SON, J. S. & HANRATTY, T. J. 1969 *J. Fluid Mech.* **35**, 369.

SQUIRE, H. B. 1934 *Phil. Mag.* **17**, 1150.

SYCHEV, V. V. 1967 *Symposium on Modern Problems in Fluid and Gas Dynamics*. Tarda, Poland.

TAKAMI, H. & KELLER, H. B. 1969 *Phys. Fluids Suppl.* II, **12**, II–51.

TANEDA, S. 1956 *J. Phys. Soc. Japan*, **11**, 302.

THOM, A. 1928 *Aero. Res. Counc. R. & M.* no. 1194.

THOM, A. 1933 *Proc. Roy. Soc.* A **141**, 651.

THOMAN, D. C. & SZEWCZYK, A. A. 1966 *Heat Transfer and Fluid Mech. Lab., University of Notre Dame Tech. Rep.* no. 66–14.

TRITTON, D. J. 1959 *J. Fluid Mech.* **6**, 547.

VAN DYKE, M. 1964 *Perturbation Methods in Fluid Mechanics*. New York: Academic.